Research Article

Carmen Barrientos*, Miguel Sanz-Novo, Clara Isabel Sánchez, Antonio Largo and Pilar Redondo

Theoretical insights on the structure and stability of the [C2, H3, P, O] isomeric family

https://doi.org/10.1515/pac-2025-0467
Received March 26, 2025; accepted June 12, 2025

Abstract: Phosphorus is a crucial biogenic element, yet its astrochemical role remains poorly understood due to its low cosmic abundance and the limited number of detected P-containing molecules in the interstellar medium. Given its significance for prebiotic chemistry, PCO-bearing molecules, such as the phosphorus analogs of isocyanates, are promising candidates for laboratory and interstellar studies. Herein, we present a comprehensive theoretical study on the isomeric landscape of the C_2H_3PO system, identifying and characterizing 24 low-lying isomers through high-level quantum chemical calculations. The study employs double-hybrid DFT and coupled-cluster methods to refine energy values and structural parameters, while topological analysis of electronic density characterizes chemical bonding. Vinylphosphinidene oxide (CH_2CHPO) emerges as the most stable isomer, followed by methylphosphaketene (CH_3PCO), with oxygen-bound structures playing a crucial role in stability. Comparisons with the C_2H_3NO system reveal structural parallels, reinforcing the importance of oxygen-bound species. Cyclic structures were also explored, with three- and four-membered P- and O-heterocycles identified, although they are generally less stable than open-chain isomers. These results provide insights into the chemical behavior and stability of C_2H_3PO isomers, which could help future spectroscopic studies and detection efforts in the interstellar medium.

Keywords: C_2H_3PO isomers; phosphorus-bearing molecules; quantum chemical calculations; quantum science and technology.

Introduction

Astrochemistry stands as a prime example of a scientific discipline where quantum chemistry plays a foundational role. The extreme conditions of the interstellar medium (ISM), with temperatures as low as a few kelvin and extremely low particle densities, present significant challenges for experimental investigations. As a result, quantum chemical calculations have become essential for advancing our understanding of chemical processes in space. From elucidating reaction mechanisms to predicting spectroscopic signatures, quantum chemistry provides critical insights into the structure and reactivity of interstellar species. Moreover, modern quantum chemistry methods routinely achieve “chemical accuracy” and are steadily approaching “spectroscopic

Article note: A collection of invited papers to celebrate the UN’s proclamation of 2025 as the International Year of Quantum Science and Technology.

***Corresponding author: Carmen Barrientos**, Departamento de Química Física y Química Inorgánica, Universidad de Valladolid, 47011 Valladolid, Spain, e-mail: carmen.barrientos@uva.es. https://orcid.org/0000-0003-0078-7379
Miguel Sanz-Novo, Centro de Astrobiología (CAB), INTA-CSIC, Carretera de Ajalvir km 4, Torrejón de Ardoz, 28850 Madrid, Spain
Clara Isabel Sánchez, Antonio Largo and Pilar Redondo, Departamento de Química Física y Química Inorgánica, Universidad de Valladolid, 47011 Valladolid, Spain

accuracy". In the context of the International Year of Quantum Science and Technology (IYQ), this study highlights the continued importance of quantum chemical tools in unraveling the molecular complexity of space.

In recent times, the study of third-row elements, particularly phosphorous (P) and sulfur (S), has garnered significant interest from the astrochemical community. Alongside carbon (C), hydrogen (H), oxygen (O) and nitrogen (N), these elements are essential for the development of life (CHONPS). However, both P and S present a relatively low cosmic availability contrasted to the rest of biogenic elements (*e.g.*, solar S/C ratio $\sim 4.9 \times 10^{-2}$, S/O ratio $\sim 2.7 \times 10^{-2}$, and P/H ratio is $\sim 3 \times 10^{-7}$).[1] In this context, while the number of S-bearing molecules detected in the interstellar medium (ISM) is steadily increasing with time, highlighting for instance the latest detections of thioacetaldehyde (CH_3CHS)[2] and dimethyl sulfide (CH_3SCH_3),[3] the chemistry of P in the ISM is much less understood. Despite its importance, its molecular inventory is surprisingly limited and, to date, only seven P-containing molecules (PN, CP, HCP, PO, PO^+, C_2P and PH_3) have been conclusively found in the ISM or circumstellar shells (see *e.g.*, 4–11).

Of particular relevance is the prebiotic role of P, as it is a major player in the biochemistry of living systems. For instance, it is present in key biomolecules such as adenosine triphosphate (ATP), which functions to retain chemical energy in cells, as well as in phospholipids, crucial for cell function and communication.[12,13] However, the way the first prebiotic P-bearing species were available on our early planet is still unclear. One possibility suggests an exogenous delivery through the impact of minor bodies such as meteorites,[12,14] as supported by the observation of P-bearing species – mainly phosphorous oxide (PO) – in the data of the comet 67P/Churyumov–Gerasimenko measured with the *Rosetta* Orbiter Spectrometer for Ion and Neutral Analysis (ROSINA) instrument.[14,15] In this context, the scarce detection of P-containing compounds in space encourages researchers to suggest novel interstellar candidates to advance our understanding of P interstellar chemistry, as well as to disclose its origin.[16–20]

In this context, PCO-bearing molecules, which can be seen as the phosphorous analogues of isocyanates (*i.e.*, molecules harboring the isocyanate, –N=C=O, functional group), together with its structural isomers and derivatives, appear as promising candidates for both laboratory and interstellar study since their chemistry is poorly understood. The NCO family, on the contrary, has received considerable attention, as these compounds are involved in the formation of amino acids, the polymerization of peptides,[21] and the synthesis of nucleotides and nucleosides.[22] Several NCO-bearing species have been discovered in the ISM, highlighting isocyanic acid (HNCO),[23–30] its cationic counterpart, H_2NCO^+,[31] the NCO radical[32] and two derivatives: methyl isocyanate (CH_3NCO)[33–37] and ethyl isocyanate (CH_3CH_2NCO).[38] An isomer of methyl isocyanate, glycolonitrile ($HOCH_2CN$), has been recently discovered in the ISM toward the Solar-type protostar IRAS16293–2422 B.[39] This molecule plays a significant role as a precursor of potential prebiotic species and facilitates the formation of other various species involved in the synthesis of life's building blocks. Moreover, its detection strongly suggests studying its corresponding P-analogue emphasizes the importance of exploring alternative structural arrangements of atoms with the same chemical formula as these [C2, H3, N, O] isomers.

In a recent work,[40] we have explored through high-level quantum-chemical computations the most stable isomers within the [CH_3, P, C, O] family, *i.e.*, CH_3PCO (global minimum in energy), CH_3OCP, CH_3CPO, CH_3COP and CH_3OPC. However, other structural isomers merit further attention. In this study, we use theoretical methods to characterize the most relevant isomers on the singlet Potential Energy Surface (PES). Herein, we analyze the structure and stability of the remaining P-bearing molecules, which stand as the very last piece in the puzzle of this somewhat exotic isomeric family. These results will also be compared with those obtained previously for analogous nitrogen-containing systems, enabling a deeper comparison between the chemistry of phosphorus and nitrogen. In this context, various theoretical studies have been conducted to characterize [C2, H3, N, O] isomers,[41–44] providing a set of theoretically predicted geometries that can assist in the detection and characterization of new molecules in the ISM. Furthermore, the data reported here will be useful for guiding eventual laboratory searches for the aforementioned systems and, ultimately, to shed further light on the interstellar chemistry of phosphorus.

Computational methods

We characterized the possible [C2, H3, P, O] isomers using density functional theory (DFT) and *ab initio* methodologies. To identify stationary points on the potential energy surface (PES), we initially optimized molecular

geometries at the DFT level. Specifically, we selected the B3LYP hybrid exchange-correlation functional,[45,46] which combines the Lee–Yang–Parr correlation functional [47] with Becke's hybrid exchange functional.[48] Subsequently, in this context, we employed the double-hybrid B2PLYP-D3 functional,[49] which integrates Hartree–Fock exchange with a perturbative second-order correlation term, alongside Grimme's D3BJ empirical dispersion correction.[50] This approach enhances accuracy in describing electronic interactions. This method is employed in conjunction with Dunning's correlation-consistent triple-zeta basis sets, aug-cc-pVTZ,[51,52] which incorporate both polarization and diffuse functions for all elements.

Furthermore, to refine the computed structural parameters and energy values of stationary points, we employ explicitly correlated coupled-cluster theory at the CCSD(T)-F12b level,[53] combined with the cc-pVTZ-F12 basis set.[54] This high-level methodology ensures an accurate treatment of electron correlation effects, crucial for obtaining precise geometries and energies. To assess the reliability of the single-reference coupled-cluster approach, we evaluated the T1 diagnostic at the CCSD(T) level,[55] obtaining values around 0.015 for all studied isomers. Since systems are generally well described by a single-reference wavefunction when the T1 diagnostic remains below 0.02,[56] our calculations confirm the robustness of this approach for the investigated species. Our previous work[57] has shown that the CCSD(T)-F12b/cc-pVTZ-F12 level of theory yields energies and geometries in excellent agreement with those obtained using a "composite" scheme, which accounts for corrections for basis set truncation error, diffuse functions, and core–valence correlation while maintain a lower computational cost. It should be also pointed out that the accuracy of the CCSD(T)-F12 method depends on several factors, including the chemical nature of the system under study, the property being calculated, and the basis set employed. Numerous benchmark studies have assessed the performance of CCSD(T)-F12b for energetic calculations, confirming its reliability and efficiency. As an example, the accuracy of atomization energies computed using CCSD(T)-F12b generally ranges from ±0.5 to ±1.0 kcal/mol, depending on the size and complexity of the molecule as well as the basis set used.[53]

We computed harmonic vibrational frequencies at their respective levels of theory for the optimized geometries. This analysis allowed us to confirm that the obtained structures correspond to true minimum on the PES and to determine zero-point vibrational (ZPV) energy corrections, which are essential for accurate thermodynamic predictions.

Beyond structural and energetic analyses, we explored the nature of chemical bonding within the [C2, H3, P, O] isomers through a topological analysis of the electronic density. We conducted this analysis within the framework of Bader's Quantum Theory of Atoms in Molecules (QTAIM),[58,59] using the AIMAll package,[60] which applies standard computational thresholds. QTAIM provided valuable insights into electron density distributions, revealing the fundamental interactions governing molecular stability and reactivity. The QTAIM analysis was performed employing the electronic density computed at the CCSD/aug-cc-pVTZ level using geometries optimized at the CCSD(T)-F12b/cc-pVTZ-F12 level. We assessed the accuracy of the integration over the atomic basin (Ω) by evaluating the magnitude of the corresponding Lagrangian function, L(Ω) (–1/4 times the atomic integral of the Laplacian of the electron density), which remained below 10^{-4} au in all cases. In the QTAIM framework, atomic interactions can be broadly classified into two limiting types: shared interactions and closed-shell interactions. Shared interactions, typical of covalent bonds, arise from the concentration of electronic charge between nuclei, leading to a lowering of potential energy. This is reflected in relatively high values of ρ(r) and a negative Laplacian ($\nabla^2\rho(r)$) at the bond critical point (BCP). In contrast, closed-shell interactions occur in systems such as ionic bonds and van der Waals complexes. These interactions are characterized by low values of ρ(r) and a positive Laplacian ($\nabla^2\rho(r)$), indicating electron depletion in the bonding region. Another key parameter for assessing bond covalency is the total energy density H(r), defined as the sum of the potential energy density V(r) and the kinetic energy density G(r) at a critical point. Covalent interactions are associated with negative H(r) values, whereas positive H(r) values are indicative of ionic or van der Waals interactions. Additionally, the |V(r)|/G(r) ratio provides a quantitative measure of bond covalency. A value greater than 2 corresponds to covalent bonds, while a value below 1 is characteristic of non-covalent interactions. Partially covalent bonds fall within the intermediate range of 1–2. A detailed discussion on the significance of various magnitudes used in QTAIM can be found in the work of Cremer and Kraka.[61]

We performed all electronic structure calculations, using computational chemistry software packages GAUSSIAN 16 [62] and MOLPRO.[63] These state-of-the-art tools ensure a comprehensive and accurate computational characterization of the investigated molecular species.

Results and discussion

We explored various potentially stable C_2H_3PO isomers, considering both open-chain and ring structures. Our selection process combined insights from previous studies on the analogous C_2H_3NO system,[41–44] information from the SciFinder database and chemical intuition. To refine our list, we excluded high-energy bicyclic structures. In the ISM, most detected compounds with multiple isomers correspond to the thermodynamically most stable form for a given chemical formula. Following the Minimum Energy Principle (MEP), we focused on isomers within 100 kcal/mol of the most stable structure, identifying a total of 24 low-lying isomers. We have included the results of our previously studied [CH_3, C, P, O] isomers [40] for an overall view.

To explore the conformational landscape of each isomer, we examined possible conformers on their respective singlet potential energy surfaces (PES). When multiple conformers were possible, only the most stable one was considered in our list of [C2, H3, P, O] isomers.

Isomeric panorama, structure, and stability

In the initial stage, we conducted a comprehensive search for plausible molecular structures that align with the [C2, H3, P, O] formula using the B3LYP functional. This search identified four distinct isomeric families as true energy minima, characterized by the presence of $-CH_3$, $-CH_2$, $-CH$, $-PH_2$, and $-PH_3$ groups. Additionally, we considered the possible existence of $HOCH_2PC$ and CH_3POC; however, both were found to be unstable on the singlet potential energy surface. For greater accuracy, we refined both the geometry and energy calculations using the B2PLYPD3/aug-cc-pVTZ and CCSD(T)-F12b/cc-pVTZ-F12 levels of theory.

Table 1 presents the relative energies of the [C2, H3, P, O] isomers, including zero-point vibrational (ZPV) corrections, computed at the B2PLYP-D3 and CCSD(T)-F12b levels of theory. The 24 optimized structures are ranked in ascending order of relative stability based on CCSD(T)-F12b calculations. Figures 1–4 displays the structural parameters of these isomers, obtained using the same computational methods.

As inferred from Figs. 1–4, both B2PLYP-D3 and CCSD(T)-F12b methodologies generally yield similar geometries. The most significant discrepancies are observed in the P–O bond lengths, where the B2PLYP-D3 formalism tends to predict longer values compared to the coupled-cluster method. For instance, this trend is evident in the P–O bond distances of the c-OPC-CH_3 (XVII) and CH_2CPOH (V) isomers, as shown in Figs. 1 and 2A, respectively.

According to our CCSD(T)-F12b calculations, the five most stable C_2H_3PO isomers are CH_2CHPO (I), CH_3PCO (II), PH_2CHCO (III), OCHCHPH (IV) and CH_2CPOH (V). This stability order remains unchanged, except for the first two isomers, CH_2CHPO (I) and CH_3PCO (II), whose relative stability is inverted when using the B2PLYP-D3 methodology. Overall, the application of the coupled-cluster method leads to a stabilization of the lowest-lying isomer compared to the B2PLYP-D3 formalism (see Table 1).

In the following discussion of our results, we will use the numerical values obtained at the CCSD(T)-F12b level of theory unless stated otherwise.

Based on our calculations the most stable isomer on the C_2H_3PO PES is vinylphosphinidene oxide, CH_2CHPO (I). As depicted in Fig. 2A, the lowest-energy conformer adopts a *trans*-CCPO conformation, where the vinyl group (CH_2=CH–) is bonded to the phosphinidene oxide (PO) unit through phosphorus, forming a CCP bond angle of 116.2°. The PO moiety, analogous to a nitrene (-N=) group, forms a CPO bond angle of 108.4°. The *cis*-CCPO conformer is slightly less stable, lying 1.6 kcal/mol higher in energy. The notable properties of nitroso compounds have driven significant research into the structural and conformational stability of various nitroso R–N=O derivatives. In this context, extensive studies have explored the structure and stability of nitrosoethylene (CH_2CHNO).[64–67] Based on microwave spectroscopy[64,65] and theoretical calculations,[66,67] nitrosoethylene is

Table 1: Relative energies (in kcal/mol) for the [C2, H3, P, O] isomers calculated at the B2PLYPD3/aug-cc-pVTZ and CCSD(T)-F12b/cc-pVTZ-F12 levels. ZPV energies estimated at the same levels are included.

Isomer	ΔE/B2PLYP-D3	ΔE/CCSD(T)-F12b
I CH_2CHPO ($^1A'$)	0	0
II CH_3PCO ($^1A'$)	−0.9	3.0
III PH_2CHCO ($^1A'$)	6.0	9.9
IV OCHCHPH ($^1A'$)	12.3	14.5
V CH_2CPOH ($^1A'$)	14.0	14.8
VI OPH_2CCH ($^1A'$)	21.2	17.6
VII CH_2PCHO ($^1A'$)	16.6	18.5
VIII $HOCH_2CP$ (^1A)	21.7	23.8
IX c-$PHCH_2C$-O (^1A)	21.1	23.9
X c-OPHC-CH_2 (^1A)	26.7	28.5
XI c-CH_2OCHP ($^1A'$)	29.4	30.1
XII CH_3OCP ($^1A'$)	27.8	31.0
XIII c-PCH_2C-OH ($^1A'$)	29.4	31.3
XIV c-PCHCH-OH (^1A)	34.0	34.8
XV $OCCPH_3$ ($^1A'$)	32.1	35.5
XVI HOCHCPH (^1A)	34.1	36.1
XVII c-OPC-CH_3 ($^1A'$)	33.6	36.9
XVIII PH_2CCOH ($^1A'$)	38.5	40.9
XIX c-CH_2OC-PH ($^1A'$)	39.9	42.1
XX CH_3CPO ($^1A'$)	45.6	44.2
XXI HCPHCHO ($^1A'$)	69.8	71.2
XXII CH_2PCOH ($^1A'$)	71.0	71.6
XXIII CH_3COP ($^1A'$)	92.3	91.9
XXIV CH_3OPC ($^1A'$)	96.9	94.6

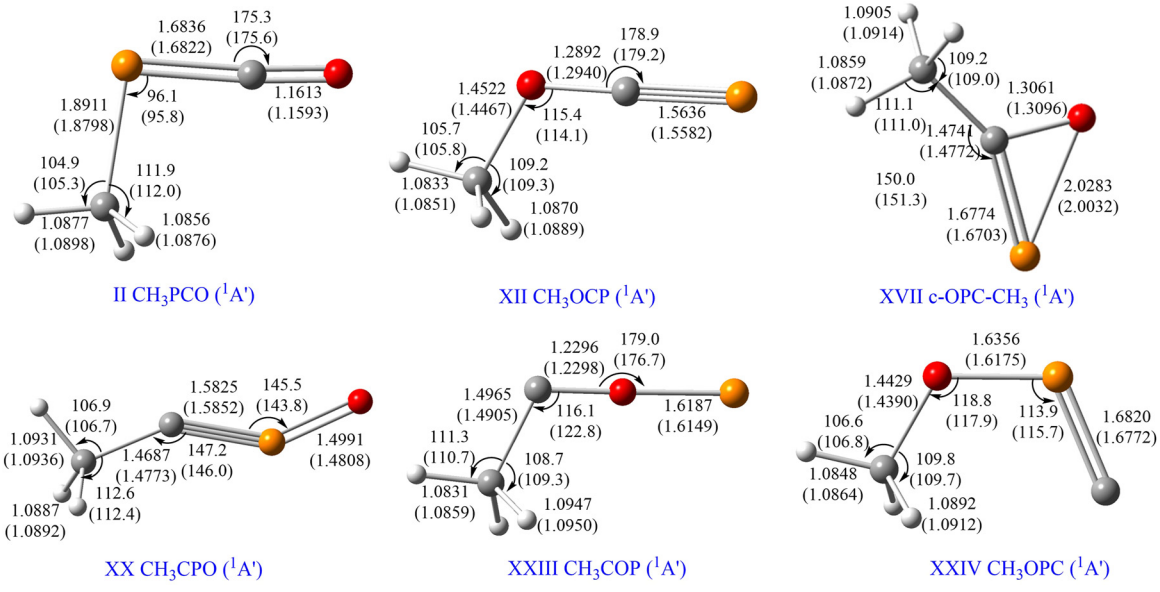

Fig. 1: Optimized geometrical parameters (in angstroms and degrees) of the [CH_3, P, C, O] isomers located at the B2PLYP-D3/aug-cc-pVTZ and CCSD(T)-F12b/cc-pVTZ-F12 (in parentheses) levels of theory. Color code: Carbon atoms are depicted in gray; oxygen atoms are in red; phosphorus atoms are in orange and hydrogen atoms are in white. Open-chain isomer geometries were taken from our previous work.[40]

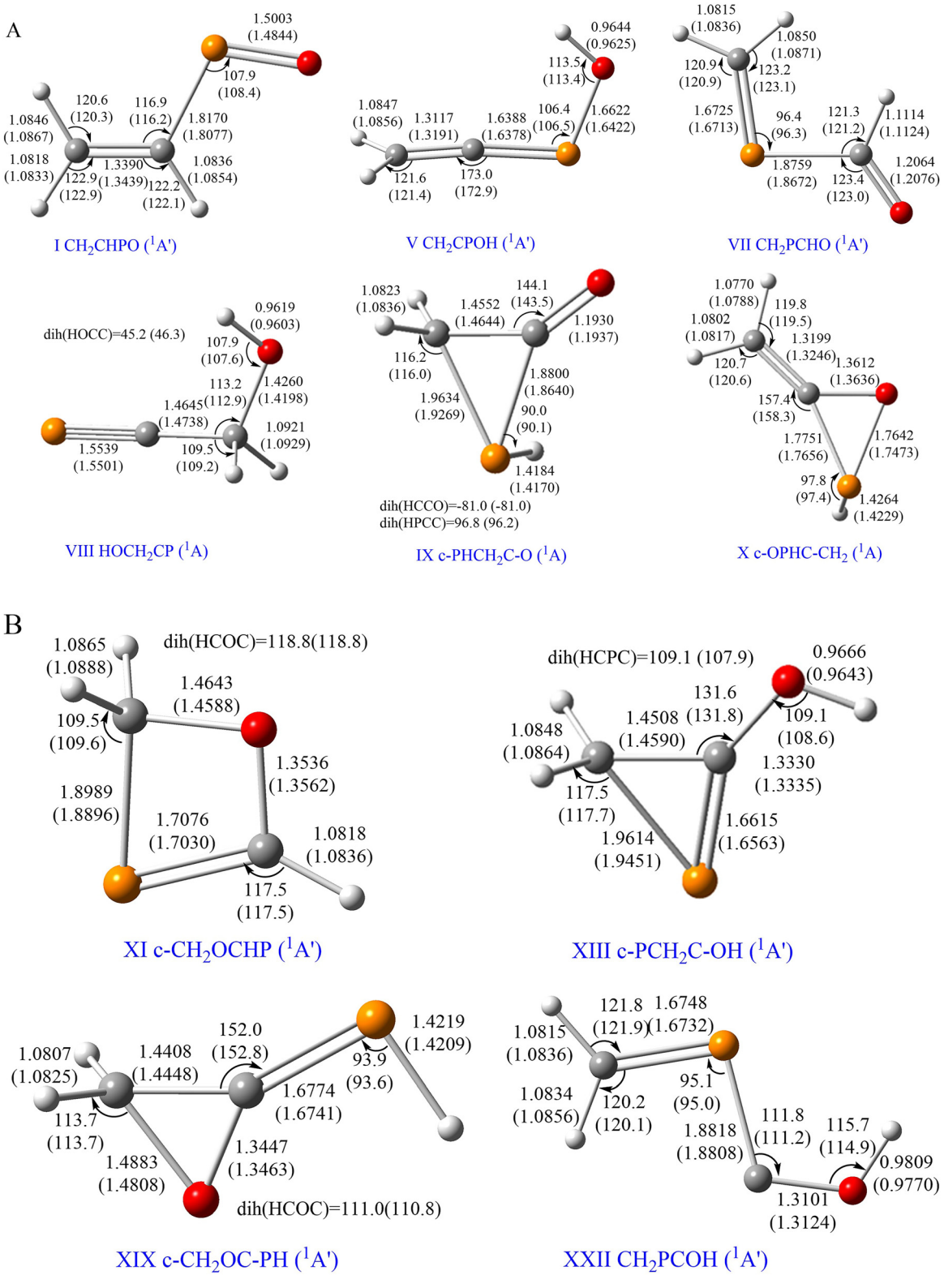

Fig. 2: Optimized geometrical parameters (in angstroms and degrees) of the [CH_2, H, P, C, O] isomers located at the B2PLYP-D3/aug-cc-pVTZ and CCSD(T)-F12b/cc-pVTZ-F12 (in parentheses) levels of theory. Color code: Carbon atoms are depicted in gray; oxygen atoms are in red; phosphorus atoms are in orange and hydrogen atoms are in white. (A) lowest lying isomers. (B) rest of isomers.

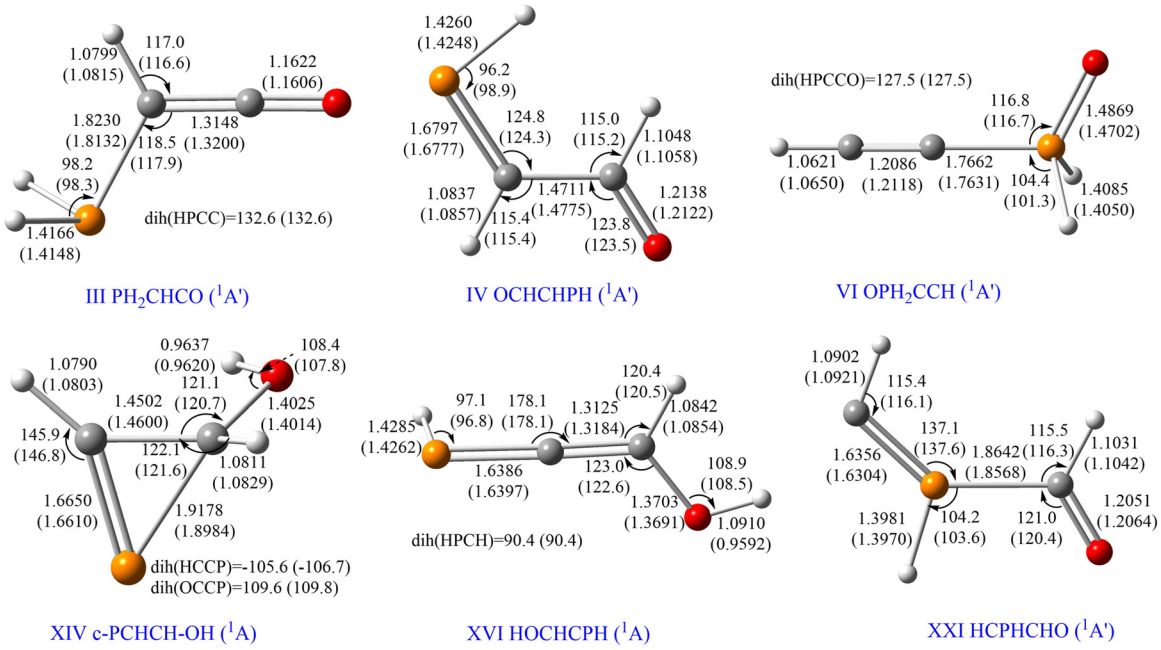

Fig. 3: Optimized geometrical parameters (in angstroms and degrees) of the [CH, H2, P, C, O] isomers located at the B2PLYPD3/aug-cc-pVTZ and CCSD(T)-F12b/cc-pVTZ-F12 (in parentheses) levels of theory. Color code: Carbon atoms are depicted in gray; oxygen atoms are in red; phosphorus atoms are in orange and hydrogen atoms are in white.

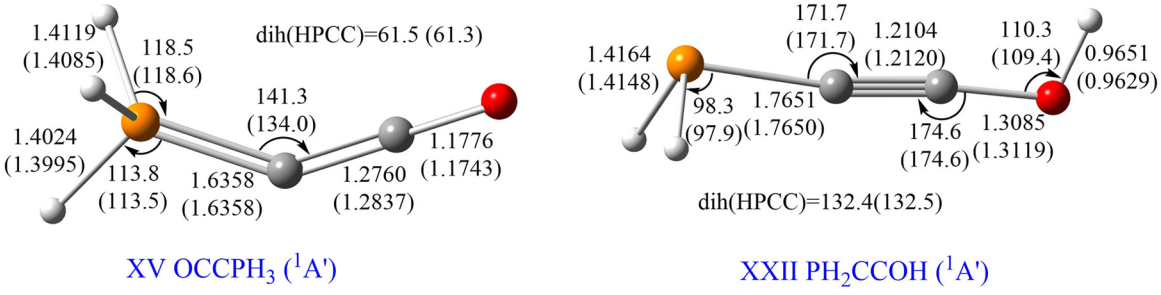

Fig. 4: Optimized geometrical parameters (in angstroms and degrees) of the XV $OCCPH_3$ and XXII PH_2CCOH isomers located at the B2PLYP-D3/aug-cc-pVTZ and CCSD(T)-F12b/cc-pVTZ-F12 (in parentheses) levels of theory. Color code: Carbon atoms are depicted in gray; oxygen atoms are in red; phosphorus atoms are in orange and hydrogen atoms are in white.

predicted to predominantly adopt a planar *trans* configuration. Computational studies at the B3LYP/6-311+G(d,p) level predict the *cis* conformer to be 4.604 kcal/mol higher in energy than the *trans* counterpart.[66] Although this *cis-trans* energy gap is significantly larger than that observed in the analogous phosphorus-containing conformers, CH_2CHPO and CH_2CHNO exhibit similar structural features. The latter displays bond angles of ∠CCN = 117.1° and ∠CNO = 112.65°, [64,65] highlighting its close structural relationship to its phosphorus-bearing counterpart.

Next in stability is methylphosphaketene CH_3PCO (II) which is situated 3.0 kcal/mol above CH_2CHPO. In this structure (see Fig. 1) the methyl (-CH_3) group links to the phosphaketene (–PCO) moiety, forming a ∠CPC angle of 95.8°. This isomer is the phosphorus analog of methyl isocyanate (CH_3NCO), a species previously detected in the ISM.[33–37] The most significant difference between the structural parameters of CH_3PCO and its analogue CH_3NCO lies in the angle formed between the two carbon atoms and either N or P. In the CH_3NCO isomer, this angle is ∠CNC = 175.6°,[61] whereas in CH_3PCO, it is significantly smaller (∠PCO = 95.8°) (see Fig. 1).

The third most stable isomer, (phosphino)methyl ketene, PH_2CHCO (III), consists of a phosphino (–PH_2) group bonded to a methyl ketene (–CHCO) moiety at carbon, forming a PCC bond angle of 117.9° (see Fig. 3). This isomer lies 9.9 kcal/mol above CH_2CHPO in energy. In contrast, its nitrogen-bearing analogue, 2-aminoethenone, NH_2CHO, is significantly less stable, positioned 27.3 kcal/mol[43] (28.66 kcal/mol)[44]) above the most stable isomer, CH_3NCO.

The fourth isomer in energy is (phosphanyl)acetaldehyde OCHCHPH (IV), in which the phosphanyl (-PH) group is bonded to the acetaldehyde (–CHCHO) moiety via the phosphorus atom (see Fig. 3). For this structure, we explored four conformers. The most stable conformer corresponds to an antiperiplanar (ap) arrangement in which the oxygen atom and the PH group lie on opposite sides of the plane, containing the C–C bond, which is perpendicular to the molecular plane, and the hydrogen atom of the PH group is addressed in the direction of the skeleton of the molecule (in). Thus, the lowest-energy isomer could be named as in-ap-(phosphanyl)acetaldehyde and lies 14.5 kcal/mol higher in energy than CH_2CHPO. The corresponding out-ap arrangement is just 0.8 kcal/mol higher in energy, while the two synperiplanar (sp) conformers lie 2.0 kcal/mol (out-sp-OCHCHPH) and 3.1 kcal/mol (in-sp-OCHCHPH) above the global minimum. The nitrogen analog, imineacetaldehyde, OCHCHNH, lies 24.19 kcal/mol above the global C_2H_3NO minimum.[44] In comparison to the most stable OCHCHPH conformer, imine acetaldehyde, OCHCHNH, adopts an out-ap arrangement.[68]

Hydroxyethynylphosphine, CH_2CPOH (V), is the fifth most stable isomer on the C_2H_3PO potential energy surface (PES), lying 14.8 kcal/mol above the global minimum. Notably, this isomer is nearly isoenergetic with OCHCHPH (IV). The lowest-energy conformer (see Fig. 2A) adopts a structure featuring a cumulene-like (CH_2=C=) backbone bonded to a phosphonyl (–P–OH) group, resulting in an OPC bond angle of 97.4° in a *in*-HOPC arrangement. The *out*-HOPC conformer is slightly less stable, lying 1.2 kcal/mol higher in energy. Hydroxyethynylphosphine is the phosphorus analog of N-hydroxyethenimine, CH_2CNOH, which is situated 66.4 kcal/mol above the global minimum CH_3NCO.[43] In contrast to CH_2CPOH, the nitrogen analog adopts a *out*-HONC arrangement.

Notably, the four most stable isomers of the C_2H_3PO potential energy surface (PES) feature the oxygen atom in a terminal position, either as part of the phosphoryl group (–P=O) in isomer I, the isophosphinate group (–PCO) in isomer II, the ketene group (–C=C=O) in isomer III, or the aldehyde group (–CHO) in isomer IV. At the opposite extreme in relativity are the isomers with either a carbon atom (isomer XXIV) or a phosphorus atom (isomer XXII) in a terminal position.

As mentioned above, several theoretical studies have explored the potential energy landscape of C_2H_3NO.[41–44] A recent study, at the RIJCOSX72-M062X/def2-TZVP level of theory, by Panda et al.[44] identified methyl isocyanate (CH_3NCO) as the most stable isomer on the C_2H_3NO PES, in agreement with the findings of Sumathi et al.,[41] Dalbouha et al.,[42] and Fourré et al.[43] According to Panda et al.' study,[44] the next most stable isomers are, 2-hydroxyacetonitrile, $HOCH_2CN$, N-methyleneformamide, CH_2NCHO, 2-imineacetaldehyde, HNCHCHO, and methylcyanate, CH_3OCN which are located 15.95, 22.55, 24.19 and 26.94 kcal/mol above the global minimum CH_3NCO, respectively. A similar stability order was found by Fourré et al. :[43] $CH_3NCO > NCCH_2OH > HNCHCHO \approx CH_2NCHO > CH_3OCN$ (where ">" indicates greater stability). At the highest level of theory used in their study (CCSD(T)/aug-cc-pVTZ//B3LYP/aug-cc-pVTZ), HNCHCHO and CH_2NCHO are isoenergetic. However, the authors suggest that N-methyleneformamide should be targeted in searches for the ISM due to its larger dipole moment.

Notably, nitrosoethylene (CH_2CHNO), the nitrogen analog of our lowest-energy C_2H_3PO isomer, does not appear in Panda et al. 's[44] list of stable isomers and was identified as a high-energy species, lying 65.1 kcal/mol above CH_3NCO in the study by Fourré et al.[43] at the CCSD(T)/aug-cc-pVTZ//B3LYP/aug-cc-pVTZ level of theory.

As mentioned earlier, the two detected C_2H_3NO isomers, that is, methyl isocyanate (CH_3NCO)[33–37] and 2-hydroxyacetonitrile ($HOCH_2CN$)[39] rank in first and second positions on the stability scale. The phosphorus analog of $HOCH_2CN$, hydroxy(methylene)phosphinidene $HOCH_2CP$ (VIII), features a hydroxymethyl group (HO–CH_2–) attached to a phosphinidene (–C≡P) structure via carbon atom. It adopts a *gauche* conformation in its lowest-energy structure and lies 23.8 kcal/mol above CH_2CHPO (I). The *trans*-conformer is only 1.3 kcal/mol higher in energy than the *gauche* form. Additionally, *gauche*-$HOCH_3CP$ is 20.8 kcal/mol less stable than CH_3PCO (II), a relative energy difference comparable to that between CH_3NCO and $HOCH_2CN$ (12.7 kcal/mol,[43] 15.95 kcal/mol [44]).

Among the 24 isomers analyzed in our study, we identified seven apparently cyclic compounds composed of three- and four-membered P- and O-heterocycles. Three of these structures feature a three-membered

P-heterocyclic core (PCC): c-PHCH$_2$C-O (IX), c-PCH$_2$C-OH (XIII), and c-PCHCH-OH (XIV). One structure exhibits a three-membered O-heterocyclic core (OCC): c-CH$_2$OC-PH (XIX). Additionally, two structures contain both P- and O-heterocyclic frameworks (POC): c-OPHC-CH$_2$ (X) and c-OPC-CH$_3$ (XVII). Lastly, one structure features a four-membered ring: c-CH$_2$OCHP (XI).

The most stable cyclic isomer, 1-phosphacyclopropan-2-one, c-PHCH$_2$C-O (IX), features a three-membered P-heterocyclic core (PCC) and is positioned 23.9 kcal/mol above CH$_2$CHPO (I) in energy. Notably, its nitrogen-containing analogue, aziridine-2-one, was also identified as the most stable cyclic structure in the C$_2$H$_3$PO potential energy surface (PES), lying approximately 35 kcal/mol above the global minimum.[43,44] All the cyclic structures analyzed in this study are relatively stable, with their energies spanning an interval of approximately 18 kcal/mol. The stability ordering for the cyclic isomers from most to less stable is as follows:

c-PHCH$_2$C-O (IX) (CCP) > X-c-OPHC-CH$_2$(CPO) > XI-c-CH$_2$OCHP(CPCO) > XIII-c-PCH$_2$C-OH(CCP) > XIV-c-PCHCH-OH(CCP) > XVII-c-OPC-CH$_3$(CPO) > XIX-c-CH$_2$OC-PH (CCO)

In this context, we recently explored the [CH$_3$, P, C, O] isomeric family,[40] analyzing five isomers with a bent heavy-atom skeleton: CH$_3$PCO, CH$_3$OCP, CH$_3$CPO, CH$_3$COP, and CH$_3$OPC. In this work, we expand the isomeric family by including a cyclic structure with a –CH$_3$ group, c-OPC-CH$_3$ (XVII), which exhibits relatively high stability. It is positioned 36.9 kcal/mol above the most stable structure, CH$_2$CHPO (I). Consequently, the –CH$_3$ isomeric family now comprises six structures (see Fig. 1) with significant differences in stability, including the second most stable isomer, CH$_3$PCO (II), and the highest-energy isomer, CH$_3$OPC (XXIV), which lies 94.6 kcal/mol above the global minimum, CH$_2$CPOH (I). The resulting stability order is as follows: CH$_3$PCO (II) > CH$_3$OCP (XII) > c-OPC-CH$_3$ (XVII) > CH$_3$CPO (XX) > CH$_3$COP (XXIII) > CH$_3$OPC (XXIV). Notably, this energetic trend aligns well with previously reported results for the analogous CH$_3$NCO isomers,[42] which follow the order: CH$_3$NCO > CH$_3$OCN > CH$_3$CNO > CH$_3$ONC.

Regarding the [CH$_2$, H, P, C, O] isomeric family, we have analyzed 10 structures (see Fig. 2A and B), including both open-chain and cyclic arrangements. Within this group, the CH$_2$ group appears in different positions: at a terminal position in open-chain structures, as seen in CH$_2$CHPO (I), CH$_2$CPOH (V), CH$_2$PCHO (VII), and CH$_2$PCOH (XXII); at an intermediate position in the open-chain structure, as in HOCH$_2$CP (VIII); and in cyclic isomers, either outside the ring, as in c-OPHC-CH$_2$ (X), or as part of the cyclic framework, as in c-PHCH$_2$CO (IX), c-CH$_2$OCHP (XI), c-PCH$_2$COH (XIII), and c-CH$_2$OCPH (XIX). This isomeric family spans an energy range of approximately 71 kcal/mol and include the global minimum CH$_2$CHPO (I) and the four-membered ring structure c-CH$_2$OCHP (XI), which is located 30.1 kcal/mol above the most stable isomer. The stability order for this family is as follows: CH$_2$CHPO (I) > CH$_2$CPOH (V) > CH$_2$PCHO (VII) > HOCH$_2$CP (VIII) > c-PHCH$_2$CO (IX) > c-OPHCCH$_2$ (X) > c-CH$_2$OCHP (XI) > c-PCH$_2$COH (XIII) > c-CH$_2$OCPH (XIX) > CH$_2$PCOH (XXII).

Within the [CH, H2, P, C, O] isomeric family, we have studied six isomers (see Fig. 3) covering an energy range of approximately 61 kcal/mol. The HC group appears at the end of the open-chain structure in OCHCHPH (IV), OPH$_2$CCH (VI), and HCPHCHO (XXI); within the structure in PH$_2$CHCO (III) and HOCHCPH (XVI); and as part of the cyclic framework in c-PCHCHOH (XIV). The stability order for this group of isomers is as follows: PH$_2$CHCO (III) > OCHCHPH (IV) > OPH$_2$CCH (VI) > c-PCHCHOH (XIV) > HOCHCPH (XVI) > HCPHCHO (XXI).

Finally, we have studied two isomers containing either a –PH$_3$ or a –PH$_2$ group (see Fig. 4): phosphapropadienone, OCCPH$_3$, (XV) and phosphanylethynol, PH$_2$CCOH, (XVIII), which are located 35.5 and 40.9 kcal/mol above the global minimum CH$_2$CHPO (I), respectively. OCCPH$_3$ (XV) features a ketene (–C=C=O) moiety bonded to a phosphine group, –PH$_3$, via a carbon atom, while PH$_2$CCOH (XVIII) consists of a phosphanyl (-PH$_2$) group connected to an ethynol (–C≡C–OH) backbone.

In summary, nitrogen and phosphorus both belong to Group 15 of the periodic table, but their chemistry differs significantly due to differences in electronegativity, atomic size, bonding behavior, and reactivity. Nitrogen is significantly more electronegative than phosphorus, resulting in more polar nitrogen bonds and stronger hydrogen bonding. In contrast, phosphorus favors single and double bonds over multiple bonding due to its larger atomic size and lower π-orbital overlap efficiency. Thus, we observe significant differences between the isomers containing nitrogen and phosphorus. The five most stable C$_2$H$_3$NO isomers – CH$_3$NCO, NCCH$_2$OH, HNCHCHO, CH$_2$NCHO, and CH$_3$OCN – span an energy range of approximately 27 kcal/mol.[43,44] In contrast, the potential energy surface (PES) of C$_2$H$_3$PO exhibits a smaller energy gap among the five lowest-energy isomers, with OCHCHPH (I) lying only about 15 kcal/mol above CH$_2$CHPO (V). Additionally, only two low-energy isomers, CH$_3$PCO (II) and

OCHCHPH (IV), have nitrogen analogs among the five lowest-energy C_2H_3PO isomers. Furthermore, unlike certain families of compounds including C_2H_3NO isomers where structures with single or double NO bonds are never among the most thermodynamically stable,[43] the lowest-energy C_2H_3PO isomer features a double P=O bond.

Bonding analysis

The nature of the bonding for the five most stable isomers and the cyclic structures was characterized by using topological analysis of the electronic charge density. This analysis identifies critical points in the one-electron density ρ(r), providing insight into the actual connectivity of each species. For the isomers studied in this work, only bond critical points (BCPs) and ring critical points (RCPs) are relevant.

The main results of the QTAIM analysis are summarized in Table 2 and 3 whereas the contour maps of the Laplacian of the electron density including the molecular graph of the isomers are presented in Figs. 5 and 6.

Table 2: Local topological properties (in au) of the electronic charge density distribution calculated at the CCSD/aug-cc-pVTZ//CCSD(T)-F12b/cc-pVTZ-F12 level, at the position of the bond critical points (BCPS) for the five lowest-lying [C2, H3, P, O] isomers.

Type	Atoms	$\rho(r)$	$\nabla^2\rho(r)$	$\lvert V(r)\rvert/G(r)\rvert$	$H(r)$
			I CH_2CHPO ($^1A'$)		
BCP1	C2 – P6	0.168	−0.045	2.069	−0.173
BCP2	C1 – C2	0.350	−1.237	4.075	−0.458
BCP3	C1 – H4	0.294	−1.187	8.350	−0.344
BCP4	C1 – H3	0.292	−1.166	8.161	−0.339
BCP5	C2 – H5	0.289	−1.147	7.933	−0.335
BCP6	P6 – O7	0.229	1.528	1.325	−0.184
			II CH_3PCO ($^1A'$)		
BCP1	O1 – C2	0.461	0.386	1.898	−0.852
BCP2	C2 – P3	0.158	0.591	1.457	−0.124
BCP3	P3 – C4	0.147	−0.216	2.600	−0.144
BCP4	C4 – H5	0.284	−1.097	7.058	−0.328
BCP5	C4 – H6	0.287	−1.118	7.247	−0.333
BCP6	C4 – H7	0.287	−1.118	7.247	−0.333
			III PH_2CHCO ($^1A'$)		
BCP1	C1 – C2	0.331	−0.609	2.404	−0.529
BCP2	C2 – O3	0.460	0.299	1.919	−0.847
BCP3	C1 – P4	0.151	0.020	1.966	−0.145
BCP4	C1 – H5	0.283	−1.091	6.996	−0.327
BCP5	P4 – H6	0.165	−0.006	2.009	−0.167
BCP6	P4 – H7	0.165	−0.006	2.009	−0.167
			IV OCHCHPH ($^1A'$)		
BCP1	C1 – C2	0.280	−0.835	4.692	−0.286
BCP2	C1 – O3	0.414	−0.100	2.035	−0.743
BCP3	C1 – H4	0.288	−1.143	9.145	−0.326
BCP4	C2 – H5	0.291	−1.157	8.089	−0.337
BCP5	C2 – P6	0.187	0.376	1.656	−0.179
BCP6	P6 – H7	0.163	−0.028	2.045	−0.164
			V CH_2CPOH ($^1A'$)		
BCP1	P1 – O2	0.164	0.681	1.428	−0.127
BCP2	P1 – C3	0.188	0.563	1.549	−0.171
BCP3	O2 – H4	0.363	−2.651	9.738	−0.748

Table 2: (continued)

Type	Atoms	$\rho(r)$	$\nabla^2\rho(r)$	$\lvert V(r)\rvert/G(r)\rvert$	$H(r)$
BCP4	C3 – C5	0.358	−1.287	3.844	−0.496
BCP5	C5 – H6	0.289	−1.153	8.028	−0.336
BCP6	C5 – H7	0.289	−1.153	8.028	−0.336

$\rho(r)$, Electronic charge density; $\nabla^2\rho(r)$, Laplacian of electronic charge density; $|V(r)|/G(r)$, Relationship between the local kinetic energy density $G(r)$ and the local potential energy density $V(r)$; $H(r)$, Total energy density.

Table 3: **L**ocal topological properties (in au) of the electronic charge density distribution calculated at the CCSD/aug-cc-pVTZ//CCSD(T)-F12b/cc-pVTZ-F12 level, at the position of the bond critical points (BCPs) for [C2, H3, P, O] isomers with a cyclic arrangement.

Type	Atoms	$\rho(r)$	$\nabla^2\rho(r)$	$\lvert V(r)\rvert/G(r)\rvert$	$H(r)$
IX c-PHCH$_2$C-O (^{1}A)					
BCP1	C1 – C2	0.280	−0.783	3.995	−0.294
BCP2	C2 – P4	0.143	−0.191	2.538	−0.136
BCP3	C2 – O3	0.427	0.120	1.963	−0.772
BCP4	C1 – P4	0.130	−0.199	2.799	−0.112
BCP5	C1 – H5	0.286	−1.116	7.349	−0.331
BCP6	C1 – H6	0.287	−1.129	7.512	−0.333
BCP7	P4 – H7	0.163	−0.002	2.003	−0.163
RCP	C1 C2 P4	0.120	0.017		
X c-OPHC-CH$_2$ (^{1}A)					
BCP1	C2 – P4	0.157	0.007	1.988	−0.156
BCP2	C1 – C2	0.352	−1.186	3.349	−0.516
BCP3	C1 – H7	0.289	−1.146	7.655	−0.337
BCP4	C2 – O3	0.295	−0.413	2.290	−0.459
BCP5	O3 – P4	0.135	0.432	1.493	−0.105
BCP6	P4 – H5	0.169	−0.068	2.107	−0.175
BCP7	C1 – H6	0.291	−1.162	7.651	−0.342
RCP	C2 O3 P4	0.131	0.382		
XI c-CH$_2$OCHP (^{1}A′)					
BCP1	C1 – P2	0.145	−0.093	2.197	−0.141
BCP2	C1 – O3	0.242	−0.499	2.576	−0.342
BCP3	P2 – C4	0.176	0.404	1.616	−0.162
BCP4	O3 – C4	0.301	−0.414	2.274	−0.481
BCP5	C4 – H5	0.299	−1.235	9.428	−0.350
BCP6	C1 – H6	0.293	−1.174	8.268	−0.340
BCP7	C1 – H7	0.293	−1.174	8.268	−0.340
RCP	C1 P2 C4 O3	0.083	0.331		
XIII c-PCH$_2$C-OH (^{1}A′)					
BCP1	C1 – C2	0.276	−0.747	3.793	−0.291
BCP2	C2 – O3	0.308	−0.347	2.212	−0.497
BCP3	C2 – P4	0.174	0.511	1.547	−0.154
BCP4	C1 – H5	0.289	−1.136	7.481	−0.336
BCP5	C1 – H6	0.289	−1.136	7.481	−0.336
BCP6	O3 – H7	0.366	−2.704	10.299	−0.758
XIV c-PCHCH-OH (^{1}A)					
BCP1	C1 – C2	0.278	−0.736	3.751	−0.289
BCP2	C2 – P4	0.136	−0.123	2.347	−0.120
BCP3	C2 – O3	0.271	−0.526	2.474	−0.409
BCP4	C1 – P4	0.178	0.439	1.600	−0.165

Table 3: (continued)

Type	Atoms	$\rho(r)$	$\nabla^2\rho(r)$	$\lvert V(r)\rvert/G(r)\rvert$	$H(r)$
BCP5	C1 – H5	0.290	−1.158	8.073	−0.337
BCP6	C2 – H6	0.300	−1.218	8.539	−0.351
BCP7	O3 – H7	0.369	−2.667	9.565	−0.755
RCP	C1 C2 P4	0.135	0.023		
		XVII c-OPC-CH$_3$ (^{1}A′)			
BCP1	C1 – C2	0.275	−0.829	4.542	−0.289
BCP2	C2 – P3	0.177	0.398	1.624	−0.165
BCP3	C2 – O4	0.336	−0.497	2.289	−0.554
BCP4	C1 – H5	0.288	−1.133	7.523	−0.335
BCP5	C1 – H6	0.283	−1.096	7.319	−0.326
BCP6	C1 – H7	0.283	−1.096	7.319	−0.326
		XIX c-CH$_2$OC-PH (^{1}A′)			
BCP1	C1 – C2	0.276	−0.748	3.696	−0.297
BCP2	C1 – O3	0.228	−0.249	2.292	−0.275
BCP3	C2 – O3	0.301	−0.306	2.192	−0.474
BCP4	C2 – P4	0.174	0.514	1.541	−0.151
BCP5	P4 – H5	0.161	−0.011	2.018	−0.161
BCP6	C1 – H6	0.299	−1.226	8.844	−0.351
BCP7	C1 – H7	0.299	−1.226	8.844	−0.351
RCP	C1 C2 O3	0.221	0.237		

$\rho(r)$, Electronic charge density; $\nabla^2\rho(r)$, Laplacian of electronic charge density; $|V(r)|/G(r)$, Relationship between the local kinetic energy density $G(r)$ and the local potential energy density $V(r)$; $H(r)$, Total energy density.

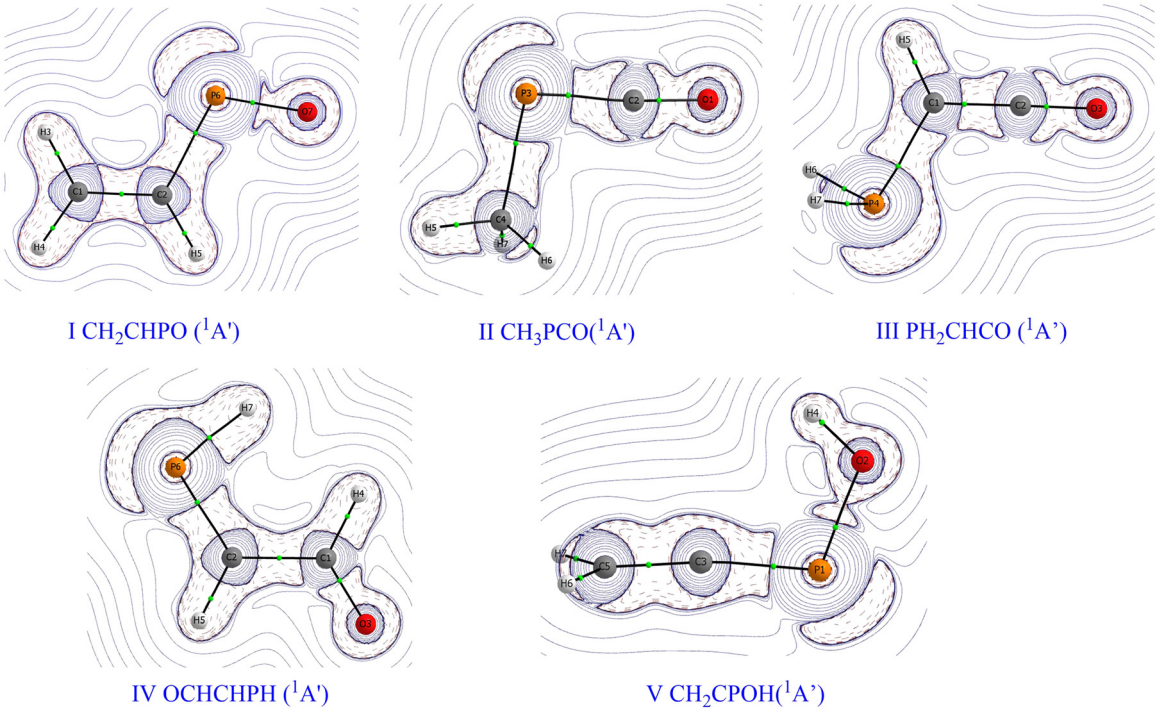

Fig. 5: Contour maps of the Laplacian distribution of the electron density for the five lowest-lying [C2, H3, P, O] isomers. Red dashed lines indicate regions of electronic charge concentration ($\nabla^2\rho(r) < 0$), and blue continuous lines denote regions of electronic charge depletion ($\nabla^2\rho(r) > 0$). Also, molecular graphs of electron density are shown, where small green spheres are bond critical points (BCPs).

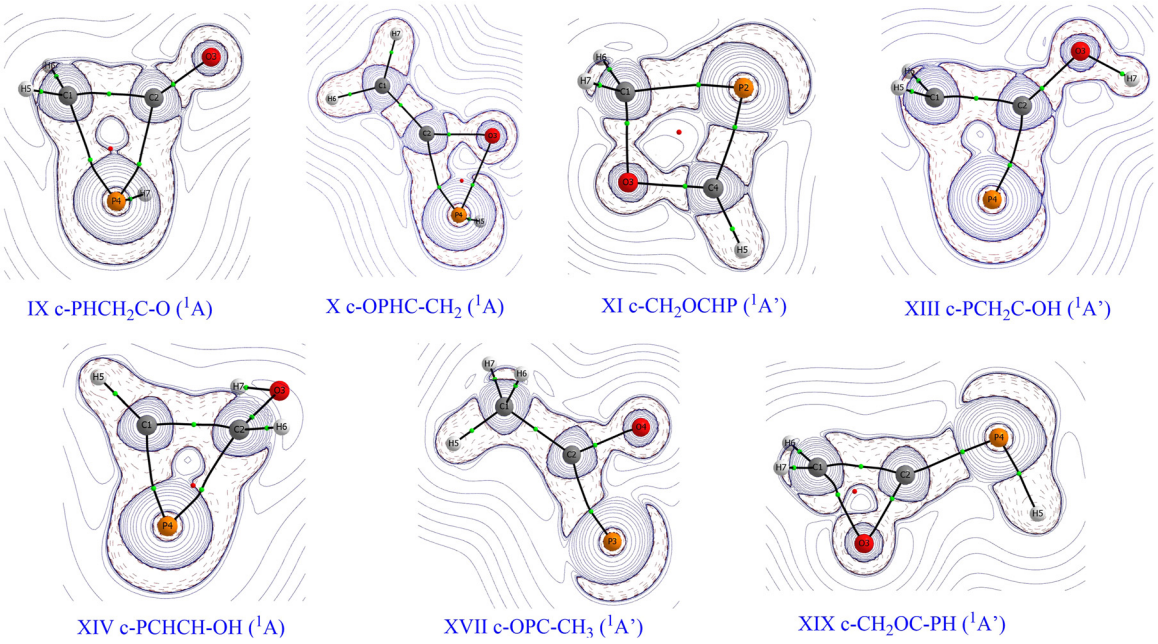

Fig. 6: Contour maps of the Laplacian distribution of the electron density for isomers with a cyclic arrangement. Red dashed lines indicate regions of electronic charge concentration ($\nabla^2\rho(r) < 0$), and blue continuous lines denote regions of electronic charge depletion ($\nabla^2\rho(r) > 0$). Also, molecular graphs of electron density are shown, where small green spheres are bond critical points (BCPs), and small red spheres are ring critical points (RCPs).

For the five lowest-lying [C2, H3, P, O] isomers (Table 2 and Fig. 5), most phosphorus-containing bonds, such as P6–O7 in CH_2CHPO (I) and P1–O2 and P1–C3 in CH_2CPOH (V), exhibit characteristics of closed-shell interactions. These bonds have relatively low electron density ρ(r) and a positive Laplacian $\nabla^2\rho(r)$, indicating electron depletion in the bonding region. However, the negative total energy densities H(r) and |V(r)|/G(r) ratios between 1 and 2 suggest a partially covalent character.

The picture emerging from the seven [C2, H3. P, O] cyclic isomers depicted in Figs. 1–3 corresponds to three- or four-membered cyclic frameworks comprising distinct ring types: These include a (PCC) ring in c-$PHCH_2C$-O (IX), c-PCH_2C-OH (XIII), and c-PCHCH-OH (XIV); an (OCC) ring in c-CH_2OC-PH (XIX); a (POC) ring in c-OPHC-CH_2 (X) and c-OPC-CH_3 (XVII); and a (COCP) ring in c-CH_2OCHP (XI). To gain deeper insight into the nature of the bonding interactions, we have employed the QTAIM framework.

For the c-$PHCH_2C$-O (IX), c-OPHC-CH_2 (X), c-CH_2OCHP (XI), c-PCHCH-OH (XIV), and c-CH_2OC-PH (XIX) isomers, the QTAIM analysis revels the presence of BCPs between all atomic pairs constituting the cyclic framework. Consequently, a RCP is identified in each case, thereby confirming the formation of true three- or four-membered ring systems.

For the *c*-PCH_2C-OH (XIII) isomer, QTAIM analysis identifies BCPs for H–C, C–C, and C–P interactions but none between C and O, preventing the detection of a RCP within the CCP framework. Likewise, in *c*-OPC-CH_3 (XVII), BCPs are found for C–P and C–O bonds, yet no direct P–O interaction is observed, precluding the formation of an RCP within the CPO skeleton. Consequently, *c*-PCH_2C-OH (XIII) and *c*-OPC-CH_3 (XVII) do not constitute true cyclic systems. Additionally, Laplacian contour maps reveal significant electron density accumulation around the phosphorus atom.

As shown in Table 3, most of the interactions analyzed exhibit characteristics of shared interactions with high electronic density values, ρ(r), and negative Laplacians, $\nabla^2\rho(r)$. Additionally, the total energy densities H(r) at the critical points are negative, indicating that the system is stabilized by the accumulation of electronic charge density in the internuclear region, a typical feature of covalent interactions. Furthermore, the |V(r)|/G(r) ratio consistently exceeds 2, further supporting the predominantly covalent nature of these interactions. However, Table 2 also highlights that most C–P bonds, such as BCPs (C2–P4) in *c*-CH_2OC-PH (XIX), P2–C4 in *c*-CH_2OCHP (XI),

C2–P4 in *c*-OPHC-CH_2 (X), C2–P4 in *c*-PCH_2C-OH (XIII), C1–P4 in *c*-PCHCH-OH, and C2–P3 in *c*-OPC-CH_3 (XVII), exhibit intermediate interaction characteristics. These bonds present positive Laplacian values and a |V(r)|/G(r) ratio between 1 and 2, indicating a predominantly covalent nature with a degree of ionic character.

For the c-OPHC-CH_2(X) isomer, the O–P bond exhibits characteristics of a closed-shell interaction with relatively low values of ρ(r) and a positive Laplacian ($\nabla^2\rho(r)$). However, the negative (though small in absolute value) total energy density H(r) and a |V(r)|/G(r) ratio between 1 and 2 suggest that this bond retains a slight degree of covalent character.

Regarding the *c*-CH_2OCHP (XI) and c-PCHCH-OH (XIV) isomers, the electron charge densities of the two C–P bonds exhibit slight variations, consistent with their optimized bond lengths. CCSD(T)-F12b/cc-pVTZ-F12 calculations yield C–P bond distances in *c*-CH_2OCHP (XI) (Fig. 2B) of d(C1–P2) = 1.8896 Å and d(P2–C4) = 1.7030 Å, with corresponding electron densities at the BCPs of 0.144549 and 0.175967, respectively. Likewise, for *c*-PCHCH-OH (XIV), the bond distances (Fig. 3) and electron charge densities are d(C2–P4) = 1.8984 Å (ρ(r) = 0.135651) and d(C1–P4) = 1.6610 Å (ρ(r) = 0.177689), following the same inverse relationship between bond length and electron charge density.

Conclusions

We systematically explored the isomeric landscape of the [C_2, H_3, P, O] system using high-accuracy quantum chemical methods. A total of 24 low-lying structures, including open-chain and three- and four-membered ring isomers, were analyzed. Our selection process combined chemical intuition, previous theoretical and experimental studies, and data-driven approaches to ensure a comprehensive assessment of plausible molecular structures. Additionally, we present a detailed topological analysis using QTAIM for the five lowest-lying and the cyclic isomers to characterize the nature of the chemical bonding. The main conclusions are the following:

- At the CCSD(T)-F12b/cc-pVTZ-F12 level, the relative stability of the five lowest-energy C_2H_3PO isomers follow the order: CH_2CHPO (I) > CH_3PCO (II) > PH_2CHCO (III) > OCHCHPH (IV) > CH_2CPOH (V). This ordering remains unchanged except for the first two isomers, CH_2CHPO (I) and CH_3PCO (II), whose relative stability is inverted when using the B2PLYPD3/aug-cc-pVTZ method.
- The most stable isomer identified in our study, employing explicit correlated coupled-cluster CCSD(T)-F12b methodology, is CH_2CHPO (I), which adopts a *trans*-CCPO conformation. This isomer exhibits close structural similarities to its nitrogen-containing counterpart, CH_2CHNO, suggesting potential chemical parallels in their formation and reactivity.
- The second most stable isomer, CH_3PCO (II), lies only 3.0 kcal/mol above CH_2CHPO and exhibits a bent PCO framework. This structural feature differentiates it from the more linear nitrogen-containing analogue, CH_3NCO, previously detected in the ISM.
- Most of the low-lying isomers feature oxygen in a terminal position, either as part of a phosphoryl (–P=O), isophosphinate (–PCO), ketene (–C=C=O), or aldehyde (–CHO) functional group, which appears to contribute significantly to the stability of these structures. In contrast, high-energy isomers, such as CH_3OPC (XXIV) and CH_2PCOH (XXII), exhibit less favorable electronic configurations, with either a terminal phosphorus or carbon atom.
- Comparisons are drawn between the C_2H_3PO system and the analogous C_2H_3NO system, in which the two most stable isomers, CH_3NCO, and $HOCH_2CN$, have been detected in the ISM. The phosphorus analog of $HOCH_2CN$, $HOCH_2CP$, was found to be in our study significantly less stable than the global minimum CH_2PHNO. Notably, CH_2CHNO, the nitrogen analog of our lowest-energy isomer CH_2CHPO, is a high-energy species in the C_2H_3NO PES, located 65.1 kcal/mol above CH_3NCO. This suggests that while CH_2CHPO is the preferred structure in the phosphorus system, its nitrogen counterpart is significantly less stable.
- Among the 24 isomers, we identified seven cyclic structures, primarily featuring three- and four-membered P- and O-heterocycles. Overall, our study indicates that while cyclic isomers can exist within the C_2H_3PO system, they tend to be less stable than their open-chain counterparts. The energetic preference for

open-chain structures suggests that interstellar detections of C_2H_3PO species may be biased toward linear or branched molecules rather than small cyclic rings.

Further spectroscopic investigations are necessary to characterize the rotational signatures of these low-lying isomers. Additionally, laboratory synthesis and reaction pathway analyses could provide insights into the feasibility of their formation under astrophysical conditions. Future work should also explore reaction mechanisms involving C_2H_3PO species in simulated ISM environments to assess their potential formation and destruction routes. Given that the most stable C_2H_3NO isomers – CH_3NCO and $HOCH_2CN$ – have already been detected in the ISM, our results provide a strong basis for future astronomical searches targeting phosphorus-bearing counterparts. CH_2CHPO and CH_3PCO emerge as the most promising candidates for detection, given their structural stability and chemical similarity to known ISM species. As phosphorus chemistry continues to gain interest in astrochemistry, these findings contribute to a deeper understanding of its molecular diversity and potential role in prebiotic chemistry.

Acknowledgments: Financial support from the Spanish Ministerio de Ciencia e Innovación (PID2020-117742GBI00/AEI/10.13039/501100011033) is gratefully acknowledged. M. S.-N. acknowledges a Juan de la Cierva Postdoctoral Fellow proyect JDC2022-048934I, funded by the Spanish Ministry of Science, Innovation and Universities/State Agency of Research MICIU/AEI/10.13039/501100011033 and by the European Union "NextGenerationEU"/PRTR.
Research ethics: Not applicable.
Informed consent: Not applicable.
Author contributions: All authors have accepted responsibility for the entire content of this manuscript and approved its submission.
Use of Large Language Models, AI and Machine Learning Tools: None declared.
Conflict of interest: The authors state no conflict of interest.
Research funding: Ministerio de Ciencia e Innovación (PID2020-117742GBI00/AEI/10.13039/501100011033).
Data availability: Not applicable.

References

1. Asplund, M.; Grevesse, N.; Sauval, A. J.; Scott, P. The Chemical Composition of the Sun. *Ann. Rev. Astron. Astrophys.* **2009**, *47*, 481–522; https://doi.org/10.1146/annurev.astro.46.060407.145222.
2. Agúndez, M.; Molpeceres, G.; Cabezas, C.; Marcelino, N.; Tercero, B.; Fuentetaja, R.; de Vicente, P.; Cernicharo, J. Detection of Thioacetaldehyde (CH_3CHS) in TMC-1: Sulfur-Oxygen Differentiation along the Hydrogenation Sequence. *Astron. Astrophys.* **2025**, *693*, L20; https://doi.org/10.1051/0004-6361/202453459.
3. Sanz-Novo, M.; Rivilla, V. M.; Endres, C. P.; Lattanzi, V.; Jiménez-Serra, I.; Colzi, L.; Zeng, S.; Megías, A.; López-Gallifa, Á.; Martínez-Henares, A.; San Andrés, D.; Tercero, B.; de Vicente, P.; Martín, S.; Requena-Torres, M. A.; Caselli, P.; Martín-Pintado, J. On the Abiotic Origin of Dimethyl Sulfide: Discovery of Dimethyl Sulfide in the Interstellar Medium. *Astrophys. J. Lett.* **2025**, *980*, L37; https://doi.org/10.3847/2041-8213/adafa7.
4. Fontani, F. Observations of Phosphorus-Bearing Molecules in the Interstellar Medium. *Front. Astron. Space Sci.* **2024**, *11*, 1451127; https://doi.org/10.3389/fspas.2024.1451127.
5. Turner, B. E.; Bally, J. Detection of Interstellar PN – the First Identified Phosphorus Compound in the Interstellar Medium. *Astrophys. J. Lett.* **1987**, *321*, L75–L79; https://doi.org/10.1086/185009.
6. Guelin, M.; Cernicharo, J.; Paubert, G.; Turner, B. E. Free CP in IRC +10216. *Astron. Astrophys.* **1990**, *230*, L9–L11.
7. Agúndez, M.; Cernicharo, J.; Guélin, M. Discovery of Phosphaethyne (HCP) in Space: Phosphorus Chemistry in Circumstellar Envelopes. *Astrophys. J. Lett.* **2007**, *662*, L91–L94; https://doi.org/10.1086/519561.
8. Tenenbaum, E. D.; Woolf, N. J.; Ziurys, L. M. Identification of Phosphorus Monoxide ($X^2\Pi_r$) in VY Canis Majoris: Detection of the First P-O Bond in Space. *Astrophys. J.* **2007**, *666*, L29–L32; https://doi.org/10.1086/521361.
9. Halfen, D. T.; Clouthier, D. J.; Ziurys, L. M. Detection of the CCP Radical ($X^2\Pi_r$) in IRC+10216: A New Interstellar Phosphorus-Containing Species. *Astrophys. J.* **2008**, *677*, L101–L104; https://doi.org/10.1086/588024.
10. Agúndez, M.; Cernicharo, J.; Decin, L.; Encrenaz, P.; Teyssier, D. Confirmation of Circumstellar Phosphine. *Astrophys. J. Lett.* **2014**, *790*, L27; https://doi.org/10.1088/2041-8205/790/2/l27.

11. Rivilla, V. M.; García De La Concepción, J.; Jiménez-Serra, I.; Martín-Pintado, J.; Colzi, L.; Tercero, B.; Megías, A.; López-Gallifa, Á.; Martínez-Henares, A.; Massalkhi, S.; Martín, S.; Zeng, S.; De Vicente, P.; Rico-Villas, F.; Requena-Torres, M. A.; Cosentino, G. Ionize Hard: Interstellar PO^+ Detection. *Front. Astron. Space Sci.* **2022**, *9*, 829288; https://doi.org/10.3389/fspas.2022.829288.
12. Pasek, M. A.; Lauretta, D. S. Aqueous Corrosion of Phosphide Minerals from Iron Meteorites: A Highly Reactive Source of Prebiotic Phosphorus on the Surface of the Early Earth. *Astrobiology* **2005**, *5*, 515–535; https://doi.org/10.1089/ast.2005.5.515.
13. Fagerbakke, K.; Heldal, M.; Norland, S. Content of Carbon, Nitrogen, Oxygen, Sulfur and Phosphorus in Native Aquatic and Cultured Bacteria. *Aquat. Microb. Ecol.* **1996**, *10*, 15–27; https://doi.org/10.3354/ame010015.
14. Altwegg, K.; Balsiger, H.; Bar-Nun, A.; Berthelier, J. J.; Bieler, A.; Bochsler, P.; Briois, C.; Calmonte, U.; Combi, M. R.; Cottin, H.; De Keyser, J.; Dhooghe, F.; Fiethe, B.; Fuselier, S. A.; Gasc, S.; Gombosi, T. I.; Hansen, K. C.; Haessig, M.; Jäckel, A.; Kopp, E.; Korth, A.; Le Roy, L.; Mall, U.; Marty, B.; Mousis, O.; Owen, T.; Rème, H.; Rubin, M.; Sémon, T.; Tzou, C. Y.; Hunter Waite, J.; Wurz, P. Prebiotic Chemicals–Amino Acid and Phosphorus–In the Coma of Comet 67P/Churyumov-Gerasimenko. *Sci. Adv.* **2016**, *2*, e1600285; https://doi.org/10.1126/sciadv.1600285.
15. Rivilla, V. M.; Drozdovskaya, M. N.; Altwegg, K.; Caselli, P.; Beltrán, M. T.; Fontani, F.; van der Tak, F. F. S.; Cesaroni, R.; Vasyunin, A.; Rubin, M.; Lique, F.; Marinakis, S.; Testi, L.; Balsiger, H.; Berthelier, J. J.; De Keyser, J.; Fiethe, B.; Fuselier, S. A.; Gasc, S.; Gombosi, T. I.; Sémon, T.; Tzou, C. Y. ALMA and ROSINA Detections of Phosphorus-Bearing Molecules: the Interstellar Thread between Star-Forming Regions and Comets. *MNRAS* **2020**, *492*, 1180–1198; https://doi.org/10.1093/mnras/stz3336.
16. Thorne, L. R.; Anicich, V. G.; Prasad, S. S.; Huntress, W. T., Jr. The Chemistry of Phosphorus in Dense Interstellar Clouds. *Astrophys. J.* **1984**, *280*, 139–143; https://doi.org/10.1086/161977.
17. Fontani, F.; Rivilla, V. M.; Caselli, P.; Vasyunin, A.; Palau, A. Phosphorus-bearing Molecules in Massive Dense Cores. *Astrophys. J. Lett.* **2016**, *822*, L30; https://doi.org/10.3847/2041-8205/822/2/l30.
18. Rivilla, V. M.; Fontani, F.; Beltrán, M. T.; Vasyunin, A.; Caselli, P.; Martín-Pintado, J.; Cesaroni, R. The First Detections of the Key Prebiotic Molecule PO in Star-forming Regions. *Astrophys. J.* **2016**, *826*, 161.
19. Jiménez-Serra, I.; Viti, S.; Quénard, D.; Holdship, J. The Chemistry of Phosphorus-Bearing Molecules under Energetic Phenomena. *Astrophys. J.* **2018**, *862*, 128; https://doi.org/10.3847/1538-4357/aacdf2.
20. Chantzos, J.; Rivilla, V. M.; Vasyunin, A.; Redaelli, E.; Bizzocchi, L.; Fontani, F.; Caselli, P. The First Steps of Interstellar Phosphorus Chemistry. *Astron. Astrophys.* **2020**, *633*, A54; https://doi.org/10.1051/0004-6361/201936531.
21. Pascal, R.; Boiteau, L.; Commeyras, A. From the Prebiotic Synthesis of α-Amino Acids towards a Primitive Translation Apparatus for the Synthesis of Peptides. In *Prebiotic Chemistry. Topics in Current Chemistry*; Walde, P., Ed.; Springer: Berlin, Heidelberg, Vol. 259, 2005; pp. 69–122; https://doi.org/10.1007/b136707.
22. Schneider, C.; Becker, S.; Okamura, H.; Crisp, A.; Amatov, T.; Stadlmeier, M.; Carell, T. Noncanonical RNA Nucleosides as Molecular Fossils of an Early Earth—Generation by Prebiotic Methylations and Carbamoylations. *Angew Chem. Int. Ed. Engl*. **2018**, *57*, 5943–5946; https://doi.org/10.1002/anie.201801919.
23. Snyder, L. E.; Buhl, D. Interstellar Isocyanic Acid. *Astrophys. J.* **1972**, *177*, 619–623; https://doi.org/10.1086/151739.
24. Jackson, J. M.; Armstrong, J. T.; Barrett, A. H. HNCO in Molecular Clouds. *Astrophys. J.* **1984**, *280*, 608–614; https://doi.org/10.1086/162033.
25. Nguyen-Q-Rieu; Henkel, C.; Jackson, J. M.; Mauersberger, R. Detection of HNCO in External Galaxies. *Astron. Astrophys.* **1991**, *241*, L33.
26. Helmich, F. P.; van Dishoeck, E. F. Physical and Chemical Variations within the W3 Star-Forming Region. II. The 345 GHz Spectral Line Survey. *Astron. Astrophys. Suppl. Series* **1997**, *124*, 205–253.
27. Rodríguez-Fernández, N. J.; Tafalla, M.; Gueth, F.; Bachiller, R. HNCO Enhancement by Shocks in the L1157 Molecular Outflow. *Astron. Astrophys.* **2010**, *516*, A98; https://doi.org/10.1051/0004-6361/201013997.
28. Zeng, S.; Jiménez-Serra, I.; Rivilla, V.; Martín, S.; Martín-Pintado, J.; Requena-Torres, M. A.; Armijos-Abendaño, J.; Riquelme, D.; Aladro, R. Complex Organic Molecules in the Galactic Centre: the N-Bearing Family. *MNRAS* **2018**, *478*, 2962–2975.
29. Nazari, P.; van Gelder, M. L.; van Dishoeck, E. F.; Tabone, B.; van't Hoff, M. L. R.; Ligterink, N. F. W.; Beuther, H.; Boogert, A. C. A.; Caratti o Garatti, A.; Klaassen, P. D.; Linnartz, H.; Taquet, V.; Tychoniec, Ł. Complex Organic Molecules in Low-Mass Protostars on Solar System Scales. *Astron. Astrophys.* **2021**, *650*, A150; https://doi.org/10.1051/0004-6361/202039996.
30. Canelo, C. M.; Bronfman, L.; Mendoza, E.; Duronea, N.; Merello, M.; Carvajal, M.; Friaça, A. C. S.; Lepine, J. Isocyanic Acid (HNCO) in the Hot Molecular Core G331.512-0.103: Observations and Chemical Modelling. *MNRAS* **2021**, *504*, 4428–4444; https://doi.org/10.1093/mnras/stab1163.
31. Gupta, H.; Gottlieb, C. A.; Lattanzi, V.; Pearson, J. C.; McCarthy, M. C. Laboratory Measurements and Tentative Astronomical Identification of H_2NCO^+. *Astrophys. J. Lett.* **2013**, *778*, L1; https://doi.org/10.1088/2041-8205/778/1/l1.
32. Marcelino, N.; Agúndez, M.; Cernicharo, J.; Roueff, E.; Tafalla, M. Discovery of the Elusive Radical NCO and Confirmation of H_2NCO^+ in Space. *Astron. Astrophys.* **2018**, *612*, L10; https://doi.org/10.1051/0004-6361/201833074.
33. Halfen, D.; Ilyushin, V. V.; Ziurys, L. M. Interstellar Detection of Methyl Isocyanate CH3NCO in Sgr B2(N): a Link from Molecular Clouds to Comets. *Astrophys. J.* **2015**, *812*, L5; https://doi.org/10.1088/2041-8205/812/1/l5.
34. Cernicharo, J.; Kisiel, Z.; Tercero, B.; Kolesniková, L.; Medvedev, I. R.; López, A.; Fortman, S.; Winnewisser, M.; de Lucia, F. C.; Alonso, J. L.; Guillemin, J. C. A Rigorous Detection of Interstellar CH_3NCO: An Important Missing Species in Astrochemical Networks. *Astron. Astrophys.* **2016**, *587*, L4; https://doi.org/10.1051/0004-6361/201527531.
35. Ligterink, N. F. W.; Coutens, A.; Kofman, V.; Müller, H. S. P.; Garrod, R. T.; Calcutt, H.; Wampfler, S. F.; Jørgensen, J. K.; Linnartz, H.; van Dishoeck, E. F. The ALMA-PILS Survey: Detection of CH_3NCO towards the Low-Mass Protostar IRAS 16293-2422 and Laboratory Constraints on its Formation. *MNRAS* **2017**, *469*, 2219–2229; https://doi.org/10.1093/mnras/stx890.

36. Martín-Doménech, R.; Rivilla, V.; Jiménez-Serra, I.; Quénard, D.; Testi, L.; Martín-Pintado, J. Detection of Methyl Isocyanate (CH_3NCO) in a Solar-type Protostar. *MNRAS* **2017**, *469*, 2230–2234; https://doi.org/10.1093/mnras/stx915.
37. Csengeri, T.; Belloche, A.; Bontemps, S.; Wyrowski, F.; Menten, K. M.; Bouscasse, L. Search for High-Mass Protostars with ALMA Revealed up to Kilo-Parsec Scales (SPARKS) II. Complex Organic Molecules and Heavy Water in Shocks Around a Young High-Mass Protostar. *Astron. Astrophys.* **2019**, *632*, A57; https://doi.org/10.1051/0004-6361/201935226.
38. Rodríguez-Almeida, L. F.; Rivilla, V. M.; Jiménez-Serra, I.; Melosso, M.; Colzi, L.; Zeng, S.; Tercero, B.; de Vicente, P.; Martín, S.; Requena-Torres, M. A.; Rico-Villas, F.; Martín-Pintado, J. First Detection of C_2H_5NCO in the ISM and Search of Other Isocyanates towards the G+0.693-0.027 Molecular Cloud. *Astron. Astrophys.* **2021**, *654*, L1; https://doi.org/10.1051/0004-6361/202141989.
39. Zeng, S.; Quénard, D.; Jiménez-Serra, I.; Martín-Pintado, J.; Rivilla, V. M.; Testi, L.; Martín-Doménech, R. First Detection of the Pre-biotic Molecule Glycolonitrile ($HOCH_2CN$) in the Interstellar Medium. *MNRAS* **2019**, *484* (1), L43–L48.
40. Sanz-Novo, M.; Redondo, P.; Sánchez, C. I.; Largo, A.; Barrientos, C.; Sordo, J. A. Structure and Spectroscopic Insights for CH_3PCO Isomers: A High-Level Quantum Chemical Study. *J. Phys. Chem. A* **2024**, *128* (20), 4083–4091; https://doi.org/10.1021/acs.jpca.4c01370.
41. Sumathi, R.; Nguyen, H. M. T.; Nguyen, M. T.; Peeters, J. Electronic Structure Calculations on the Reaction of Vinyl Radical with Nitric Oxide. *J. Phys. Chem. A* **2000**, *104*, 1905–1914; https://doi.org/10.1021/jp993274l.
42. Dalbouha, S.; Senent, M. L.; Komiha, N.; Dominguez-Gomez, R. Structural and Spectroscopic Characterization of Methyl Isocyanate, Methyl Cyanate, Methyl Fulminate, and Acetonitrile N-Oxide Using Highly Correlated Ab Initio Methods. *J. Chem. Phys.* **2016**, *145*, 124309; https://doi.org/10.1063/1.4963186.
43. Fourre, I.; Matz, O.; Ellinger, Y.; Guillemin, J.-C. Relative Thermodynamic Stability of the [C, N, O] Linkages as an Indication of the Most Abundant Structures in the ISM. *Astron. Astrophys.* **2020**, *639*, A16; https://doi.org/10.1051/0004-6361/202037839.
44. Panda, S.; Chiranjibi, A.; Awasthi, D.; Ghosal, S.; Anoop, A. Exploring the Chemical Space of C2H3NO Isomers and Bimolecular Reactions with Hydrogen Cyanide and Formaldehyde: Insights into the Emergence of Life. *ACS Earth Space Chem*. **2023**, *7*, 1739–1752; https://doi.org/10.1021/acsearthspacechem.3c00113.
45. Becke, A. D. Density Functional Calculations of Molecular Bond Energies. *J. Chem. Phys.* **1986**, *84*, 4524–4529; https://doi.org/10.1063/1.450025.
46. Becke, A. D. A Multicenter Numerical Integration Scheme for Polyatomic Molecules. *J. Chem. Phys.* **1988**, *88*, 2547–2553; https://doi.org/10.1063/1.454033.
47. Lee, C.; Yang, W.; Parr, R. G. Development of the Colle-Salvetti Correlation-Energy Formula into a Functional of the Electron Density. *Phys. Rev. B: Condens. Matter Mater. Phys.* **1988**, *37*, 785–789; https://doi.org/10.1103/physrevb.37.785.
48. Becke, A. D. Correlation Energy of an Inhomogeneous Electron Gas: A Coordinate-Space Model. *J. Chem. Phys.* **1988**, *88*, 1053–1062; https://doi.org/10.1063/1.454274.
49. Grimme, S. J. Semiempirical Hybrid Density Functional with Perturbative Second-Order Correlation. *J. Chem. Phys.* **2006**, *124*, 034108; https://doi.org/10.1063/1.2148954.
50. Grimme, S.; Ehrlich, S.; Goerigk, L. Effect of the Damping Function in Dispersion Corrected Density Functional Theory. *J. Comput. Chem.* **2011**, *32*, 1456–1465; https://doi.org/10.1002/jcc.21759.
51. Dunning, T. H. Gaussian Basis Sets for Use in Correlated Molecular Calculations. I. The Atoms Boron through Neon and Hydrogen. *J. Chem. Phys.* **1989**, *90*, 1007–1023; https://doi.org/10.1063/1.456153.
52. Kendall, R. A.; Dunning, T. H.; Harrison, R. J. Electron Affinities of the First-Row Atoms Revisited. Systematic Basis Sets and Wave Functions. *J. Chem. Phys.* **1992**, *96*, 6796–6806; https://doi.org/10.1063/1.462569.
53. Knizia, G.; Adler, T. B.; Werner, H.-J. Simplified CCSD(T)- F12 Methods: Theory and Benchmarks. *J. Chem. Phys.* **2009**, *130*, 054104; https://doi.org/10.1063/1.3054300.
54. Peterson, K. A.; Adler, T. B.; Werner, H. J. Systematically Convergent Basis Sets for Explicitly Correlated Wavefunctions: The Atoms H, He, B-Ne, and Al-Ar. *J. Chem. Phys.* **2008**, *128*, 084102; https://doi.org/10.1063/1.2831537.
55. Lee, T. J.; Taylor, P. R. A Diagnostic for Determining the Quality of Single-Reference Electron Correlation Methods. *Int. J. Quantum Chem.* **1989**, *36*, 199–207; https://doi.org/10.1002/qua.560360824.
56. Martin, J. M. L.; Lee, T. J.; Scuseria, G. E.; Taylor, P. R. Ab Initio Multireference Study of the BN Molecule. *J. Chem. Phys.* **1992**, *97*, 6549–6556; https://doi.org/10.1063/1.463684.
57. Redondo, P.; Sanz-Novo, M.; Barrientos, C. CN and CCH Azirine Derivatives, Possible Precursors of Prebiotic Molecules: Formation and Spectroscopic Parameters. *MNRAS* **2023**, *527*, 8659–8670; https://doi.org/10.1093/mnras/stad3770.
58. Bader, R. F. W. *Atoms in Molecules. A Quantum Theory*; Clarendon Press: Oxford, U.K., 1994.
59. Fradera, X.; Austen, M. A.; Bader, R. F. W. The Lewis Model and beyond. *J. Phys. Chem. A* **1999**, *103*, 304–314; https://doi.org/10.1021/jp983362q.
60. Keith, T. A. *AIMAll, Version 13.11.04, Professional*; TK Gristmill Software: Overland Park, KS, 2013. Available from: http://aim.tkgristmill.com.
61. Cremer, D.; Kraka, E. Chemical Bonds without Bonding Electron Density – Does the Difference Electron-Density Analysis Suffice for a Description of the Chemical Bond? *Angew. Chem., Int. Ed.* **1984**, *23*, 627–628; https://doi.org/10.1002/anie.198406271.
62. Frisch, M. J.; Trucks, G. W.; Schlegel, H. B.; Scuseria, G. E.; Robb, M. A.; Cheeseman, J. R.; Scalmani, G.; Barone, V.; Petersson, G. A.; Nakatsuji, H. *Gaussian 16, Revision A.03*; Gaussian, Inc.: Wallingford, CT, 2016.
63. Werner, H.-J.; Knowles, P. J.; Celani, P.; Györffy, W.; Hesselmann, A.; Kats, D.; Knizia, G.; Köhn, A.; Korona, T.; Kreplin, D.; Lindh, R.; Ma, Q.; Manby, F. R.; Mitrushenkov, A.; Rauhut, G.; Schütz, M.; Shamasundar, K. R.; Adler, T. B.; Amos, R. D.; Baker, J.; Bennie, S. J.; Bernhardsson, A.; Berning, A.; Black, J. A.; Bygrave, P. J.; Cimiraglia, R.; Cooper, D. L.; Coughtrie, D.; Deegan, M. J. O.; Dobbyn, A. J.; Doll, K.;

Dornbach, M.; Eckert, F.; Erfort, S.; Goll, E.; Hampel, C.; Hetzer, G.; Hill, J. G.; Hodges, M.; Hrenar, T.; Jansen, G.; Köppl, C.; Kollmar, C.; Lee, S. J. R.; Liu, Y.; Lloyd, A. W.; Mata, R. A.; May, A. J.; Mussard, B.; McNicholas, S. J.; Meyer, W.; Miller, T. F.; Mura, M. E.; Nicklass, A.; O'Neill, D. P.; Palmieri, P.; Peng, D.; Peterson, K. A.; Pflüger, K.; Pitzer, R.; Polyak, I.; Pulay, P.; Reiher, M.; Richardson, J. O.; Robinson, J. B.; Schröder, B.; Schwilk, M.; Shiozaki, T.; Sibaev, M.; Stoll, H.; Stone, A. J.; Tarroni, R.; Thorsteinsson, T.; Toulouse, J.; Wang, M.; Welborn, M.; Ziegler, B. *MOLPRO*, version 2023.2, a package of *ab initio* programs, 2023.

64. Sakaizumi, T.; Usami, A.; Satoh, H.; Ohashi, O.; Yamaguchi, I. Generation and Microwave Spectrum of Trans-nitrosoethylene CH2=CH-NO. *J. Mol. Spectrosc.* **1994**, *164*, 536–549; https://doi.org/10.1006/jmsp.1994.1096.
65. Sakaizumi, T.; Nishikawa, M.; Ohashi, O. Microwave Spectrum of Trans-nitrosoethylen2-15n and Pyrolisis Mechanism of Chloroacetaldehyde Oxime. *J. Mol. Spectrosc.* **1995**, *171*, 518–524; https://doi.org/10.1006/jmsp.1995.1138.
66. Badawi, H. M.; Forner, W. Analyses of Vibrational Spectra of Nitroso- and Nitroethylenes. *J. Mol. Struct.* **2004**, *677*, 153–160; https://doi.org/10.1016/j.theochem.2004.02.037.
67. Forner, W.; Badawi, H. M. Infrared and Raman Spectra and Vibrational Analyses Calculated with Moeller–Plesset Perturbation Theory of Second Order of Nitrosoethylene and its Chloro-Derivatives. *J. Mol. Model.* **2005**, *11*, 542–550; https://doi.org/10.1007/s00894-005-0281-6.
68. Redondo, P.; Largo, A.; Barrientos, C. Structure and Spectroscopic Properties of Imine Acetaldehyde: a Posible Interstellar Molecule. *MNRAS* **2018**, *478*, 3042–3048; https://doi.org/10.1093/mnras/sty1175.